Rate coefficients of photoionization in hot dense plasmas

H. Furukawa
Institute for Laser Technology, Suita, Osaka 565, Japan
(Received 27 July 1994; revised manuscript received 13 February 1995)

The cross sections and the rate coefficients of photoionization in hot dense plasmas are estimated quantitatively by using the atomic model including electron-electron, electron-ion, and ion-ion correlations [H. Furukawa and K. Nishihara, Phys. Rev. A **46**, 6596 (1992)]. They are compared with those obtained by other models. The wave function of free states greatly affects the cross sections and the rate coefficients of photoionization considerably. It is shown that the photoionization cross sections have fine structures, especially near the threshold, which are mainly determined by the wave function of free states. The rate coefficient of photoionization obtained by the present calculation is roughly 400 times that obtained from hydrogenlike atom approximations for a set of plasma parameters: atomic number $Z=4$, ion number density $\bar{n}_i=5\times10^{22}$ cm^{-3}, plasma temperature $T=50$ eV, and photon temperature $T_{\rm ph}=10$ eV.

PACS number(s): 52.25.Kn

I. INTRODUCTION

The investigation of atomic processes in hot dense plasmas is very interesting and important for the success of inertial confinement fusion. Particle correlation effects greatly affect atomic processes in hot dense plasmas so strongly that their cross sections are quite different from those for an isolated atom system. Roughly speaking, two types of models can be adopted to calculate electronic state of atoms in hot dense plasmas. One is the detailed configuration accounting (DCA) model and the other the average atom (AA) model. It is difficult to take into account particle correlation effects in the DCA model exactly. Works along this line have been performed by Salzmann, Yin, and Pratt [1]. In order to estimate the cross sections and the rate coefficients of atomic processes in hot dense plasmas, the author constructed the atomic model based on the AA model in the previous work [2], including particle correlation effects exactly within the framework of quantal hypernetted-chain (QHNC) approximation [3]. In this paper, the cross sections and the rate coefficients of photoionization in hot dense plasmas are described. The present calculations are compared with those obtained by other models, in order to elucidate the particle correlation effects.

In Sec. II, I survey the atomic model in the previous work as well as in other models. In Sec. III, the formations of the photoionization cross sections in the AA model [4] are surveyed. And the formation of the rate coefficients of photoionization is also surveyed. In Sec. IV, the author discusses results obtained for the cross sections and the rate coefficients of photoionization in hot dense plasmas. Section V is devoted to the concluding remarks.

II. ATOMIC MODELS

In order to estimate the effects of particle correlations on photoionization in hot dense plasmas, and to clarify which effect is dominant on photoionization in hot dense plasmas quantitatively, I wish to compare six types of atomic models.

First I will explain the full-correlation atomic model indicated as FCAM, second the two-component plasma (TCP) quantal finite-temperature jellium model indicated as QJM, third the no ion-ion correlation model indicated as NIICM, fourth the jellium vacancy model indicated as JVM, fifth the jellium vacancy Thomas-Fermi model indicated as JVTFM, and sixth the ion sphere model indicated as ISM. By comparing FCAM with QJM, the free-electron–free-electron correlation effects on the photoionization are clarified. Upon comparison of QJM with NIICM and JVM, the ion-ion correlation effects on the photoionization are elucidated. Comparison of JVM with JVTFM makes clear the effects originating from different calculations of the free-electron distribution function around the ion. Finally, by comparing JVTFM with ISM, the effects originating from different boundary conditions used are clarified. Atomic units are used throughout this article unless otherwise specified.

A. Full-correlation atomic model

I will give a brief survey of the full-correlation atomic model (FCAM) expounded upon in a previous work [2]. The word "full correlation" means inclusion of all electron-electron, electron-ion, and ion-ion correlations. The effective potentials, $V_{\rm fe\text{-}fe}(r)$, $V_{\rm e\text{-}i}(r)$, and $V_{\rm i\text{-}i}(r)$, which determine the practical distribution functions, are calculated through the Ornstein-Zernike (OZ) relation within the framework of QHNC [3]. Here, the suffix fe means the free electron, e the total (free and bound) electron, and i the ion. They are given by Eqs. (2.1)–(2.3) in Ref. [2].

The direct correlation functions $c_{\mu\text{-}\nu}(r)$ are related to the μ-type particle distribution function around a test ν-type particle $n_{\mu\text{-}\nu}(r)$ through Eqs. (2.8)–(2.11) in Ref. [2]. The ion distribution function around a test ion $n_{\rm i\text{-}i}(r)$ and

the free-electron distribution function around the test free electron are obtained by Eqs. (2.18) and (2.20) in Ref. [2].

The free-electron number density and the bound-electron number density around the test ion $n_{e\text{-}i}(r)$ is obtained by solving the Schrödinger equation with $V_{e\text{-}i}(r)$

$$-\frac{1}{2}\frac{d^2\chi_{\nu,l}}{dr^2}+\left\{V_{e\text{-}i}(r)+\frac{l(l+1)}{2r^2}\right\}\chi_{\nu,l}=E\chi_{\nu,l}\ , \tag{2.1}$$

where

$$\Psi(\mathbf{r})=\sum_{l,m}\chi_{\nu,l}(r)Y_{l,m}(\theta,\phi)/r\ . \tag{2.2}$$

$\Psi(\mathbf{r})$ is the eigen-wave-function of the Schrödinger equation; $Y_{l,m}$ is the spherical harmonics. The boundary conditions required to solve Eq. (2.1) are as follows [5]. Because of the charge neutrality, $V_{e\text{-}i}(r)$ should satisfy the condition

$$rV_{e\text{-}i}(r)\underset{r=\infty}{\sim}0\ . \tag{2.3}$$

The wave function of bound states should satisfy the condition at $r=\infty$

$$\chi_{\nu,l}\approx\exp(-\sqrt{|2E|}r)\ , \tag{2.4}$$

and that of scattering (free) states should satisfy the asymptotic form

$$\Psi(\mathbf{r})\underset{r=\infty}{\sim}e^{i(\mathbf{k}\cdot\mathbf{r}+\delta)}\ , \tag{2.5}$$

where δ is the phase shift.

The electron number density around the test ion $n_{e\text{-}i}(r)$ can be obtained, using the radial wave function $\chi_{n,l}$ as

$$n_{e\text{-}i}(r)=\bar{n}_{fe}+n_{be\text{-}i}(r)+\Delta n_{fe\text{-}i}(r) \tag{2.6}$$

with

$$n_{be\text{-}i}(r)=2\sum_{n,l}\frac{(2l+1)}{4\pi}\left[\frac{\chi_{n,l}(r)}{r}\right]^2 f(E_{n,l}) \tag{2.7}$$

and

$$\Delta n_{fe\text{-}i}(r)=\sum_{l=0}^{\infty}\frac{1}{\pi^2}\int_0^{\infty}dk\,k^2 f(k^2/2)(2l+1)\times\left[\left[\frac{\chi_{k,l}(r)}{r}\right]^2-j_{k,l}^2(r)\right]\ , \tag{2.8}$$

where $j_{k,l}$ is the spherical Bessel function, $\bar{n}_{fe}$ is the average free-electron number density, $\Delta n_{fe\text{-}i}(r)$ is the displaced free electron number density, and $f(E)$ is the Fermi distribution function defined as

$$f(E)=\frac{1}{1+\exp\{\beta(E-\mu)\}}\ , \tag{2.9}$$

where $\beta=1/T$, T is the plasma temperature, and μ is the chemical potential determined in Eq. (2.15) in Ref. [2]. The ionization state Z^* is determined, using $n_{be\text{-}i}(r)$ as

$$Z^*=Z-N_{be}\ , \tag{2.10}$$

where

$$N_{be}=\int n_{be\text{-}i}(r)d\mathbf{r}\ . \tag{2.11}$$

Z is the atomic number and N_{be} is the number of bound electrons. Equations listed above are solved by iteration.

In order to accelerate a convergence, a clever choice of initial inputs is designed. In this calculation, the initial values are chosen as follows [6]. As the first step, I adopt the approximations that $c_{fe\text{-}fe}(r)=c_{fe\text{-}fe}^{jell}(r)$, $c_{fe\text{-}i}(r)\sim\beta Z^*/r$, and $h_{i\text{-}i}(r)=h_{i\text{-}i}^{OCP}(r)$ or $h_{i\text{-}i}(r)=\theta(r-a)-1$ in the OZ relation. $h_{i\text{-}i}(r)$ is the ion-ion pair correlation function and a the ion sphere radius defined as

$$a=\{3/(4\pi\bar{n}_i)\}^{1/3}\ , \tag{2.12}$$

where n_i is the average ion number density. The suffix jell stands for the jellium model and OCP means the one-component plasma. $\theta(r-a)$ is the step function defined as

$$\theta(r-a)=\begin{cases}0 & \text{for } r<a\\ 1 & \text{for } r\geq a\ .\end{cases} \tag{2.13}$$

In this approximation, the OZ relation is reduced into the form

$$\hat{h}_{fe\text{-}i}(k)=\tilde{\chi}_{fe}^0(k)\hat{c}_{fe\text{-}i}(k)+\tilde{\chi}_{fe}^0(k)\hat{\gamma}_{fe\text{-}i}(k)\ , \tag{2.14}$$

where

$$\hat{\gamma}_{fe\text{-}i}(k)=\frac{\bar{n}_{fe}\tilde{\chi}_{fe}^0(k)\hat{c}_{fe\text{-}fe}^{jell}(k)}{1-\bar{n}_{fe}\tilde{\chi}_{fe}^0(k)\hat{c}_{fe\text{-}fe}^{jell}(k)}\tilde{c}_{fe\text{-}i}(k)\ , \tag{2.15}$$

$$\tilde{c}_{fe\text{-}i}(k)=\hat{c}_{fe\text{-}i}(k)+4\pi\bar{n}_i\beta Z^*/k^2\hat{h}_{i\text{-}i}^*(k)\ , \tag{2.16}$$

$$h_{i\text{-}i}^*(r)=\theta(r-a)-1\quad\text{or}\quad h_{i\text{-}i}^*(r)=g_{i\text{-}i}^{OCP}(r)-1\ . \tag{2.17}$$

The caret stands for the Fourier transform. $\hat{c}_{fe\text{-}fe}^{jell}(k)$ is the direct correlation function obtained by the electron jellium model, $h_{fe\text{-}i}(r)$ is the free-electron–ion pair correlation function, and $\tilde{\chi}_{fe}$ is the electric susceptibility determined by Eq. (2.12) in Ref. [2]. A set of coupled Eqs. (2.14)–(2.17) is solved iteratively to obtain $c_{fe\text{-}i}$ to be used at a next step.

In the second step, a new $h_{i\text{-}i}(r)$ is calculated with the aid of the screened potential determined as

$$\beta v^{eff}(k)=4\pi\beta Z^{*2}/k^2-\hat{c}_{fe\text{-}i}(k)^2\frac{\bar{n}_{fe}\tilde{\chi}_{fe}^0(k)}{1-\bar{n}_{fe}\tilde{\chi}_{fe}^0(k)\hat{c}_{fe\text{-}fe}^{jell}(k)}\ . \tag{2.18}$$

In the third step, a new $c_{fe\text{-}i}$ is calculated by using $g_{i\text{-}i}$ and $c_{i\text{-}i}$ obtained in the second step. The second and third steps are solved iteratively.

B. TCP quantal finite-temperature jellium model [2]

When the direct correlation function between the free electrons is replaced by that of the jellium model, the OZ relation can be written as

$$\hat{h}_{\text{fe-i}}(k)-\tilde{\chi}^0_{\text{fe}}(k)\hat{c}_{\text{fe-i}}(k)=\tilde{\chi}^0_{\text{fe}}(k)\bar{n}_{\text{fe}}\hat{c}^{\text{jell}}_{\text{fe-fe}}(k)\hat{h}_{\text{fe-i}}(k)+\tilde{\chi}^0_{\text{fe}}(k)\bar{n}_{\text{i}}\hat{c}_{\text{fe-i}}(k)\hat{p}_{\text{i-i}}(k) \tag{2.19}$$

and

$$\hat{h}_{\text{i-i}}(k)-\hat{c}_{\text{i-i}}(k)=\bar{n}_{\text{fe}}\hat{c}_{\text{i-fe}}(k)\hat{h}_{\text{fe-i}}(k)+\bar{n}_{\text{i}}\hat{c}_{\text{i-i}}(k)\hat{h}_{\text{i-i}}(k)\ . \tag{2.20}$$

The set of Eqs. (2.19) and (2.20) is the same as that used in the TCP (two-component plasma) quantal finite-temperature jellium model (QJM) defined in Ref. [2]. This approximation means that the electron-ion and the ion-ion correlation functions are solved self-consistently.

C. No ion-ion correlation model

When the author adds one more assumption, that ions be distributed uniformly as the positive background, the OZ relation reduces to the form

$$\hat{h}_{\text{fe-i}}(k)-\tilde{\chi}^0_{\text{fe}}(k)\hat{c}_{\text{fe-i}}(k)=\tilde{\chi}^0_{\text{fe}}(k)\bar{n}_{\text{fe}}\times\hat{c}^{\text{jell}}_{\text{fe-fe}}(k)\hat{h}_{\text{fe-i}}(k)\ . \tag{2.21}$$

The model referring to Eq. (2.21) and Eqs. (2.2) and (2.7) in Ref. [2] is what I call the NIICM.

D. Jellium vacancy model

In Eq. (2.19), the author approximates the pair correlation function between the ions as [6]

$$h_{\text{i-i}}(r)=\theta(r-a)-1\ . \tag{2.22}$$

The model based on Eqs. (2.19) and (2.22), together with Eqs. (2.2) and (2.7) in Ref. [2], is called the jellium vacancy model (JVM).

E. Jellium vacancy Thomas-Fermi model

In the models mentioned above in Secs. II A–II D, the free-electron distribution function around the test ion is obtained as a solution to the Schrödinger equation. In this section (II E), it is calculated by Thomas-Fermi approximation as

$$n_{\text{fe-i}}(r)=\int_{E>0}\frac{2d\mathbf{k}}{(2\pi)^3}f_T(k,r)\ , \tag{2.23}$$

where

$$f_T(k,r)=\frac{1}{1+\exp[\beta\{k^2/2+V_{\text{e-i}}(r)-\mu\}]} \tag{2.24}$$

and

$$E=k^2/2+V_{\text{e-i}}(r)\ . \tag{2.25}$$

In the jellium vacancy model, when the author replaces $\hat{c}_{\text{fe-fe}}(k)$ with $-\beta 4\pi/k^2$ and $\hat{c}_{\text{fe-i}}(k)$ with $\beta 4\pi Z^*/k^2$, the electron-ion effective potential $V_{\text{e-i}}$ is related to the charge distribution functions through the Poisson equation as

$$V_{\text{e-i}}(r)=V_c(r)+\mu_{\text{xc}}[\bar{n}_{\text{fe}}+n_{\text{be-i}}(r)]-\mu_{\text{xc}}(n_{\text{fe}}) \tag{2.26}$$

and

$$\nabla^2V_c(r)=4\pi[Z^*\theta(r-a)-\{n_{\text{fe-i}}(r)+n_{\text{be-i}}(r)\}] \tag{2.27}$$

where μ_{xc} is the exchange correlation potential [7]. It is the same as that used in the above-mentioned other models. Boundary conditions are given by

$$V_c(r)\underset{r\to 0}{\sim}-\frac{Z}{r}+b \tag{2.28}$$

and

$$rV_c(r)\underset{r\to\infty}{\sim}0\ . \tag{2.29}$$

This model is called the jellium vacancy Thomas-Fermi model (JVTFM).

F. Ion sphere model

As another model, the author quotes the ion sphere model. In this model, a nuclear charge Ze is located at the center of the ion sphere of radius a and distributes electrons inside it. The effective potential $V_{\text{e-i}}$ is calculated by Eqs. (2.26) and (2.30) with the boundary conditions at $r=0$ and $r=a$, i.e.,

$$\nabla^2V_c(r)=-4\pi\{n_{\text{fe-i}}(r)+n_{\text{be-i}}(r)\} \tag{2.30}$$

with

$$V_c(r)\underset{r\to 0}{\sim}-\frac{Z}{r}+b \tag{2.31}$$

and

$$V_c(a)=\frac{d}{dr}V_c(a)=0\ . \tag{2.32}$$

The free-electron distribution function around the test ion is calculated by the Thomas-Fermi approximation. This model is called the ion sphere model. Note that this model is the same as that investigated in Ref. [8], except the exchange correlation potential, which is valid within a nonrelativistic regime. It does not include the relativistic effect which is not significant for low-Z atoms.

III. FORMATION OF THE CROSS SECTION AND THE RATE COEFFICIENT OF PHOTOIONIZATION

The photoionization cross section is related to the oscillator strength (density), defined as [4]

$$f_{ij}=(2/3)\Delta E_{ij}\left\langle\Psi_i^*(\mathbf{r})\left|\sum_{k=1}^{N}\mathbf{r}_k\right|\Psi_j(\mathbf{r})\right\rangle^2\ , \tag{3.1}$$

where ΔE_{ij} stands for the excitation energy between the levels i and j, Ψ_i and Ψ_j for the initial and final state wave functions. $\mathbf{r}_k$ is the position vector of a kth electron and N the total number of electrons.

In the average atom approximation, the oscillator strength density can be written as [4]

$$\frac{df_{nl,\alpha}}{d\varepsilon_\alpha}=\tfrac{2}{3}h\nu N_{nl}B_\alpha\left\{|D(nl,\alpha l+1)|^2\frac{l+1}{2l+1}\frac{dn^{l+1}}{d\varepsilon_\alpha}+|D(nl,\alpha l-1)|^2\frac{l}{2l+1}\frac{dn^{l-1}}{d\varepsilon_\alpha}\right\}, \tag{3.2}$$

where $D(nl,\alpha l')$ stands for the dipole integral

$$D(nl,\alpha l')=\int_0^{R_0}\chi_{nl}(r)\chi_{\alpha l'}(r)r\,dr \tag{3.3}$$

with $\chi_{\alpha l'}(r)$ the radial part of the l'th partial wave normalized over the radius R_0. Note that the orthogonality of wave functions of bound and free states is managed by the Schmidt method. N_{nl} represents the number of electrons in the shell of principal and angular momentum quantum numbers nl and is written as

$$N_{nl}=2(2l+1)/\{\exp[\beta(\varepsilon_{nl}-\mu)]+1\}\ . \tag{3.4}$$

B_α is regarded as the availability factor and has the simple form

$$B_\alpha=\frac{\exp[\beta(\varepsilon_\alpha-\mu)]}{\exp[\beta(\varepsilon_\alpha-\mu)]+1}\ . \tag{3.5}$$

Using the Bohr-Sommerfeld quantization rule, the number density of states has the form

$$\frac{dn^l}{d\varepsilon_\alpha}=\frac{1}{\pi}\int_{r_0}^{R_0}\left\{2[\varepsilon_\alpha-V_{\text{e-i}}(r)]-\frac{l(l+1)}{r^2}\right\}^{-1/2}dr\ , \tag{3.6}$$

where r_0 is the inner classical turning point. Note that, in the JVTFM and ISM, models, the radius R_0 cannot be determined self-consistently. I set $R_0=10a_e$ and $R_0=a$ to calculate the photoionization cross section within the framework of the JVTFM and $R_0=a$ to calculate the photoionization cross section within the framework of ISM. Here a_e is the electron sphere radius defined by

$$a_e=\{3/(4\pi Z\bar{n}_i)\}^{1/3}\ . \tag{3.7}$$

The indicator JVTFM in the next section means that I have set $R_0=10a_e$ to calculate the photoionization cross section within the framework of JVTFM, while the indicator JVTFM* in the next section means that I have set $R_0=a$ to calculate the photoionization cross section within the framework of JVTFM.

The cross section for the process $\varepsilon_{nl}+h\nu\rightarrow\varepsilon_{\alpha l}$ is given by

$$\sigma(\nu)=2\pi^2\frac{e^2}{\hbar c}\frac{df_{nl,\alpha}}{d\varepsilon_\alpha}a_B^2 \tag{3.8}$$

and

$$\frac{e^2}{\hbar c}=\frac{1}{137.067\,738\,2}\ , \tag{3.9}$$

where a_B is the Bohr radius and $\hbar$ is Planck's constant divided by 2π. In case of hydrogenlike atom approximation (HLAM) [9], Eq. (3.8) is rewritten as

$$\sigma(\nu)=\frac{8\pi}{3\sqrt{3}}\frac{Z^4}{n^5}\frac{e^2}{\hbar c}\frac{g_{fb}}{(h\nu)^3}a_B^2\ , \tag{3.10}$$

where g_{fb} is the Gaunt factor and the author sets $g_{fb}=0.93$.

The rate coefficient is related to the cross section as

$$A(T_{\text{ph}})=\int U(\nu)\frac{c}{h}\frac{\sigma(\nu)}{N_{n,l}}\frac{d\nu}{\nu}=\frac{c}{a_B\pi^2}\left[\frac{e^2}{\hbar c}\right]^3\int\frac{\sigma(\nu)/a_B^2}{N_{n,l}}F(h\nu)dh\nu\ . \tag{3.11}$$

$U(\nu)$ is the photon distribution function in *cgs* units, which are assumed to be Planckian in this paper. $U(\nu)$ and $F(h\nu)$ are written as

$$U(\nu)=\frac{8\pi h\nu^3}{c^3}\frac{1}{\exp(\beta h\nu)-1} \tag{3.12}$$

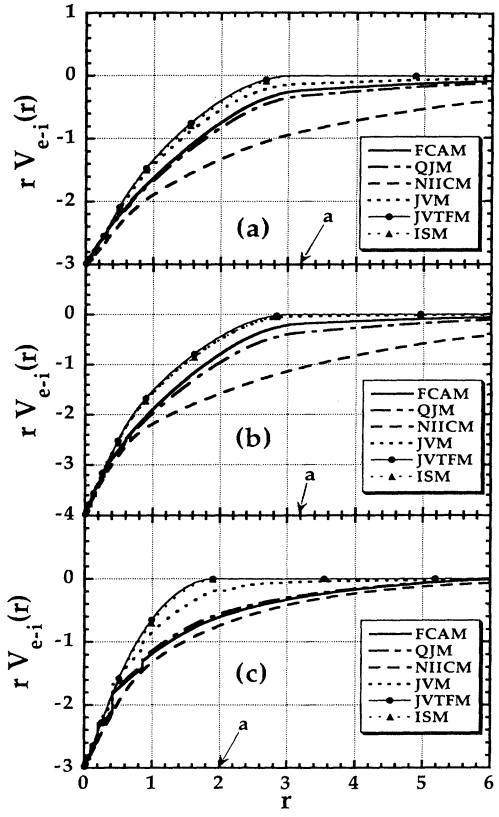

FIG. 1. The effective potentials obtained by full correlation model (FCAM), TCP quantal finite-temperature jellium model (QJM), no ion-ion correlation model (NIICM), jellium vacancy model (JVM), jellium vacancy Thomas-Fermi model (JVTFM), and ion sphere model (ISM). Part (a) corresponds to case 1, (b) to case 2, and (c) to case 3. The solid line shows the result by FCAM, the solid dotted line that by QJM, the dashed line that by NIICM, the dotted line that by JVM, the solid line with closed circles that by JVTFM, and the dotted line with the closed triangles that by ISM. The horizontal axis represents the distance from a central (test) ion and the vertical axis represents $rV_{\text{e-i}}$.

and

$$F(h\nu)=\frac{(h\nu)^2}{\exp(\beta h\nu)-1}\ . \tag{3.13}$$

IV. RESULTS AND DISCUSSIONS

A. Effective potentials and wave functions of 1s state

I carried out the calculations of photoionization cross sections using the models mentioned in previous sections for three cases. In case 1, a set of parameters used are $Z=3$, $\bar{n}_i=5\times10^{22}$ cm^{-3}, and $T=50$ eV; in case 2, $Z=4$, $\bar{n}_i=5\times10^{22}$ cm^{-3}, and $T=50$ eV; and in case 3, $Z=3$, $\bar{n}_i=2\times10^{23}$ cm^{-3}, and $T=50$ eV. In Fig. 1, the effective potentials obtained by the full correlation model (FCAM), the TCP quantal finite-temperature jellium model (QJM), the no ion-ion correlation model (NIICM), the jellium vacancy model (JVM), the jellium vacancy Thomas-Fermi model (JVTFM), and the ion sphere model (ISM) are shown. Part (a) corresponds to case 1, part (b) to case 2, and part (c) to case 3. The solid line shows the result by FCAM, the solid dotted line that by QJM, the dashed line that by NIICM, the dotted line that by JVM, the solid line with closed circles that by JVTFM, and the dotted line with closed triangles that by ISM. The horizontal axis represents the distance from a central (test) ion and the vertical axis represents $rV_{e\text{-}i}$. The mark a denotes the ion sphere radius. These results mainly reflect the differences of the treatments of the ion-ion correlation effects.

In Fig. 2, the radial part of the wave function of the 1s state for various models is shown. Parts (a), (b), and (c) have the same meaning as those in Fig. 1. The vertical axis represents $rR_{1s}(r)$. As shown in Fig. 2(a), the wave functions of the 1s state by FCAM, QJM, JVM, and JVTFM are almost the same, and because the continuum lowering effects, their values at $r\gtrsim2$ are larger than those by HLAM. The values by NIICM are slightly smaller than those by FCAM, QJM, JVM, and JVTFM. Note that the wave function by ISM reduces to zero at $r\sim3.2$ owing to the boundary condition. In Table I, the ionization state Z^* and the energy level of the 1s state ε_{1s} are shown. Due to the continuum lowering effect, each energy level of the 1s state obtained by FCAM, QJM, NIICM, JVM, JVTFM, and ISM is larger than that of HLAM. Similar tendencies are observed in Figs. 2(b) and 2(c). But in case 3, the discrepancies between the wave functions are the largest of the three cases because of a high ion number density.

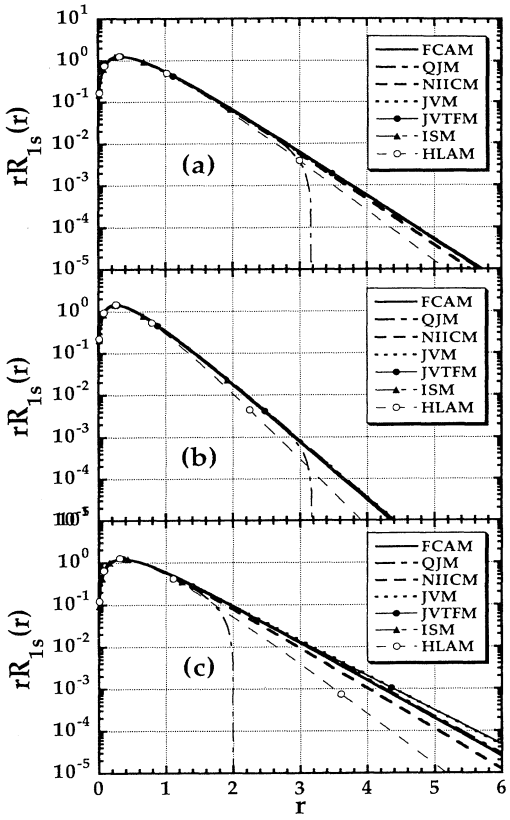

FIG. 2. The radial part of the wave function of the 1s state. Parts (a), (b), and (c) are the same as in Fig. 1. The solid line, the dash-dotted line, the dashed line, the dotted line, and the solid line with closed circles have the same meaning as in Fig. 1. The dash-dotted line with closed triangles stands for that by ISM and the dashed line with open circles stands for that by HLAM. The horizontal axis represents the distance from a central (test) ion and the vertical axis represents $rR_{1s}(r)$.

B. Photoionization cross sections

In Fig. 3, the photoionization cross section for case 1 is depicted. In Fig. 3(a), those by FCAM, ISM, and HLAM

TABLE I. Ionization state Z^* and energy level of the 1s state ε_{1s}. In case 1, $Z=3$, $\bar{n}_i=5\times10^{22}$ cm^{-3}, and $T=50$ eV; in case 2, $Z=4$, $\bar{n}_i=5\times10^{22}$ cm^{-3}, and $T=50$ eV; and in case 3, $Z=3$, $\bar{n}_i=2\times10^{23}$ cm^{-3}, and $T=50$ eV.

	Case 1		Case 2		Case 3	
	Z^*	$-\varepsilon_{1s}$	Z^*	$-\varepsilon_{1s}$	Z^*	$-\varepsilon_{1s}$
FCAM	2.544	2.902	2.937	5.106	2.169	2.171
QJM	2.537	2.942	2.936	5.110	2.179	2.120
NIICM	2.479	3.274	2.866	5.414	2.101	2.487
JVM	2.558	2.817	2.997	4.845	2.237	1.848
JVTFM	2.569	2.749	3.000	4.835	2.251	1.780
ISM	2.596	2.740	3.031	4.880	2.290	1.805
HLAM	2.000	4.500	3.000	8.000	2.000	4.500

are shown in the range of photon energy $h\nu=0\sim20$ with $\Delta h\nu=0.05$. The solid line indicates the cross section by FCAM, the solid-dotted line by ISM, and the dashed line by HLAM. The horizontal axis represents the photon energy. As shown in Fig. 3(a), each threshold of the cross sections by FCAM and ISM is smaller than that by HLAM because of the continuum lowering effects. The peak values by FCAM and ISM exist near the threshold in Fig. 3(a). In the range of $h\nu$ larger than 10, the cross sections by FCAM and ISM reach to the finite values in

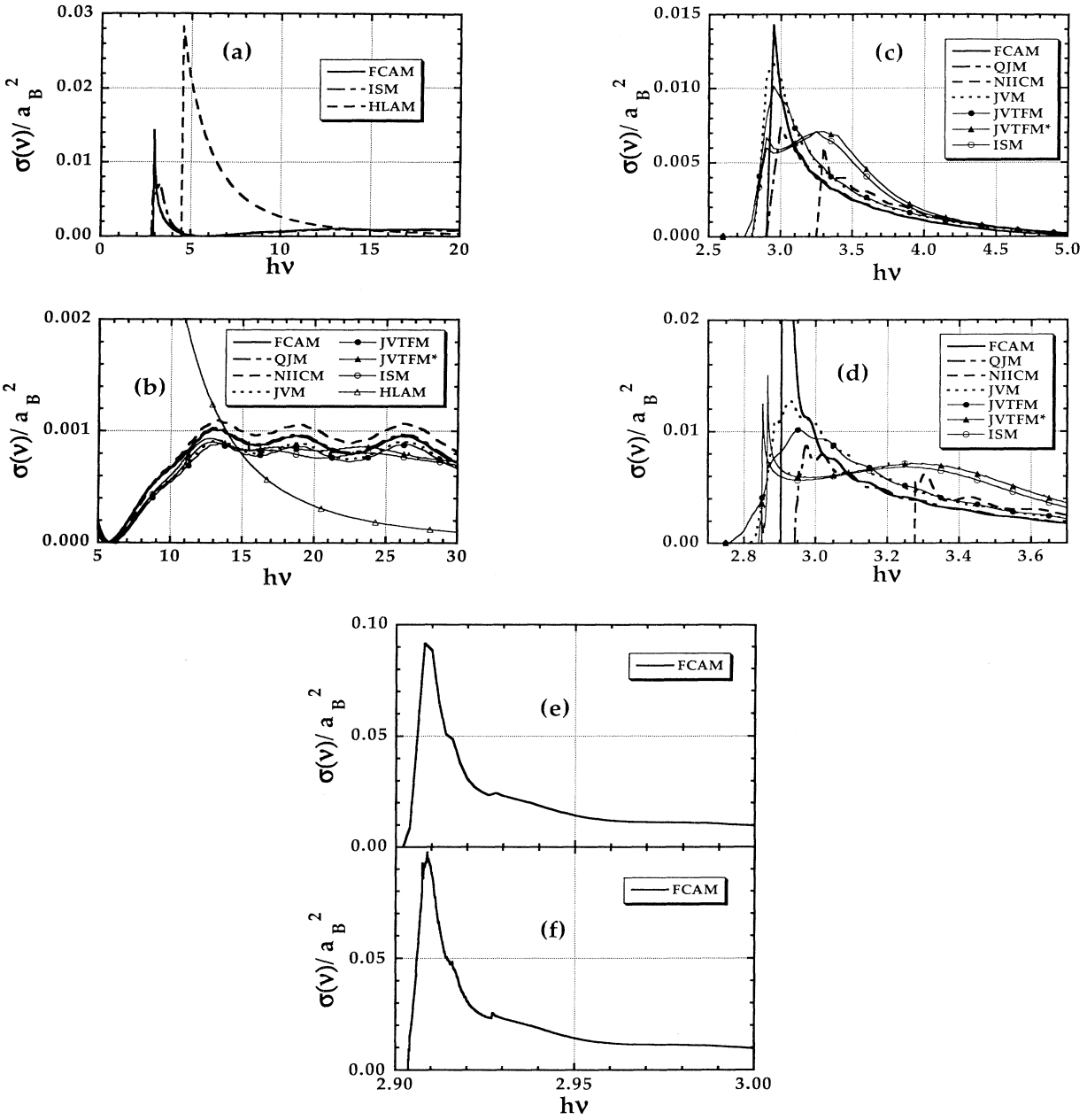

FIG. 3. (a) The photoionization cross section for case 1 by FCAM, ISM, and HLAM in the range of photon energy $h\nu=0$–20 with $\Delta h\nu=0.05$. The solid line shows that by FCAM, the dash-dotted line that by ISM, and the dashed line that by HLAM. The horizontal axis represents the photon energy. (b) The photoionization cross section in the range of $5\leq h\nu\leq30$. The solid line, the dash-dotted line, the dashed line, the dotted line, and the solid line with closed circles have the same meaning as in Fig. 1. The solid line with closed triangles stands for those by JVTFM*, the solid line with open circles stands for those by ISM, and the solid line with open triangles that by HLAM. (c) The photoionization cross section in the range of $h\nu=2.5$–5 with $\Delta h\nu=0.05$. The seven lines have the same meaning as in (b). (d) The photoionization cross section with the range of $h\nu=2.7$–3.7 with $\Delta h\nu=0.002$. The seven lines have the same meaning as in (c). (e) The photoionization cross section by FCAM in the range of $h\nu=2.9$–3.0 with $\Delta h\nu=0.002$. (f) The photoionization cross section by FCAM in the range of $h\nu=2.9$–3.0 with $\Delta h\nu=0.0002$.

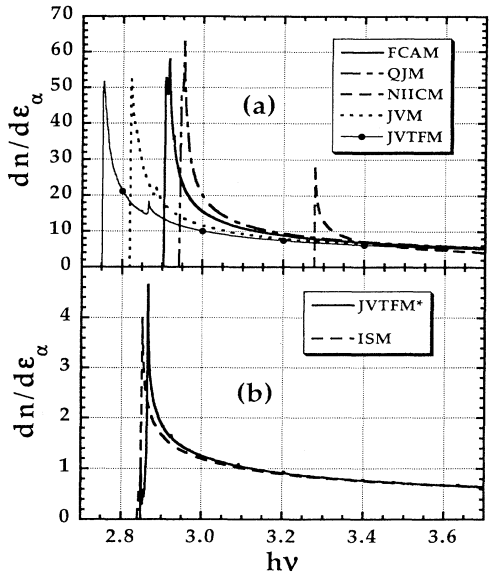

FIG. 4. (a) The number density of states obtained by FCAM, QJM, NIICM, JVM, and JVTFM defined by Eq. (3.6). The five lines have the same meaning as in Fig. 3(c). (b) The number density of states obtained by JVTFM* and ISM defined by Eq. (3.6). The solid line represents that by JVTFM* and the dashed line stands for that by ISM.

spite of the fact that by HLAM reduces to zero. In Fig. 3(b), the detailed data of the photoionization cross sections at the range of $5 \leq h\nu \leq 30$ are shown. The solid line, the dash-dotted line, the dashed line, the dotted line, and the solid line with closed circles mean the same as those in Fig. 1. The solid line with the closed triangles stands for that by JVTFM*, the solid line with open circles represents that by ISM, and the solid line with open triangles that by HLAM. Cross sections calculated by FCAM, QJM, NIICM, JVM, and JVTFM manifest almost the same oscillation period of $h\nu \sim 8$ and those by JVTFM* and ISM a period of $h\nu \sim 15$. Each amplitude of the oscillations is smaller than that of the oscillation mentioned above. These differences stem from different normalization conditions of the wave functions of free states. Figure 3(c) illustrates the photoionization cross sections with the range of $h\nu = 2.5-5$ with $\Delta h\nu = 0.05$. The seven curves have the same meaning as those in Fig. 3(b). As shown in Fig. 3(c), the photon energy dependence of the photoionization cross sections can be divided into two types. One is the existence of one peak and a subsequent decrease endowed with a small oscillation as the photon energy increases. The other is the existence of two successive peaks. These differences also originate from different normalization conditions of the wave functions of free states. Figure 3(d) shows the photoionization cross sections in the range of $h\nu = 2.7-3.7$ with $\Delta h\nu = 0.002$. The meaning of the seven lines is the same as those in Fig. 3(c). As shown in Figs. 3(c) and 3(d), the

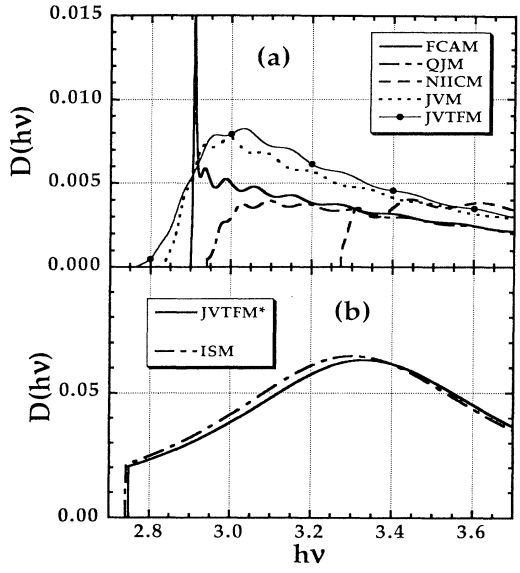

FIG. 5. (a) The dipole integrals obtained by FCAM, QJM, NIICM, JVM, and JVTFM defined by Eq. (3.3). Each line has the same meaning as in Fig. 4(a). (b) The dipole integrals obtained JVTFM* and ISM defined by Eq. (3.3). Each line has the same meaning as in Fig. 4(b).

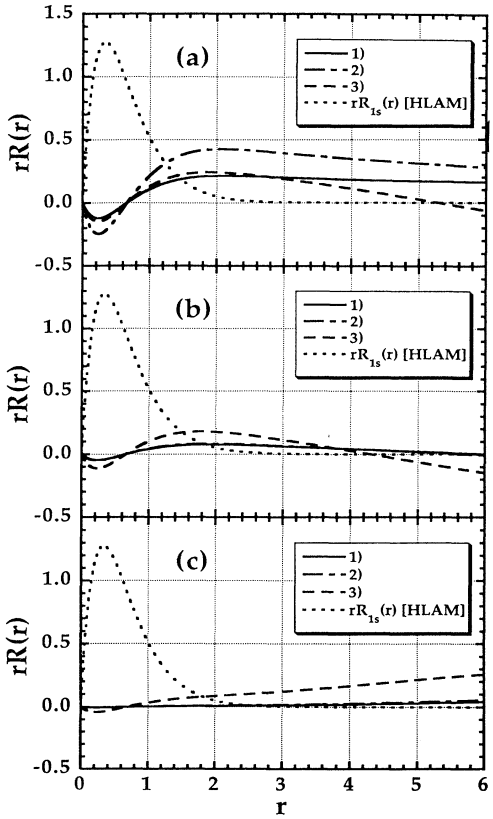

FIG. 6. (a) The wave function of free states by FCAM with the electron kinetic energy $\varepsilon_\alpha = 2.277 \times 10^{-3}$, 6.277×10^{-3}, and 0.05 and the wave function of the 1*s* state by HLAM. In (a), 1) corresponds to the case $\varepsilon_\alpha = 2.277 \times 10^{-3}$, 2) to the case $\varepsilon_\alpha = 6.277 \times 10^{-3}$, and 3) to the case $\varepsilon_\alpha = 0.05$. (b) The same as in (a) except those that are obtained by QJM. (c) The same as in (a) except those that are obtained by JVTFM.

effect of free-electron–free-electron correlation and of ion-ion correlation on peak values of the photoionization cross section are comparable except the peak value by FCAM in Fig. 3(d). In Figs. 3(c) and 3(d), the photon energy dependence of the photoionization cross section has a similar tendency, but their absolute values are different especially that by FCAM. This means that the photoionization cross section has the fine structure. Figure 3(e) shows the photoionization cross section by FCAM in the range of $h\nu=2.9-3.0$ with $\Delta h\nu=0.002$. Figure 3(f) shows the photoionization cross sections by FCAM in the range of $h\nu=2.9-3.0$ with $\Delta h\nu=0.0002$. As shown in Figs. 3(e) and 3(f), two curves behave in almost the same way. By comparing Fig. 3(e) with Fig. 3(f), one can

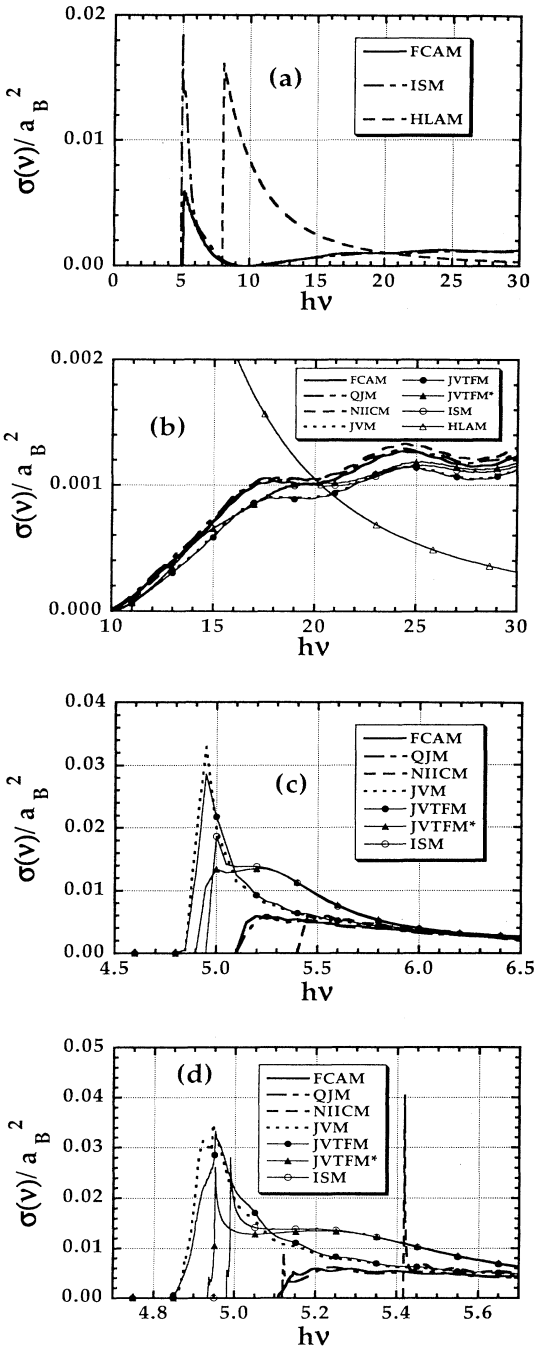

FIG. 7. (a) The photoionization cross section for case 2. All lines have the same meaning as in Fig. 3(a). (b) The photoionization cross section for case 2. All lines have the same meaning as in Fig. 3(b). (c) The photoionization cross section for case 2. All lines have the same meaning as in Fig. 3(c).

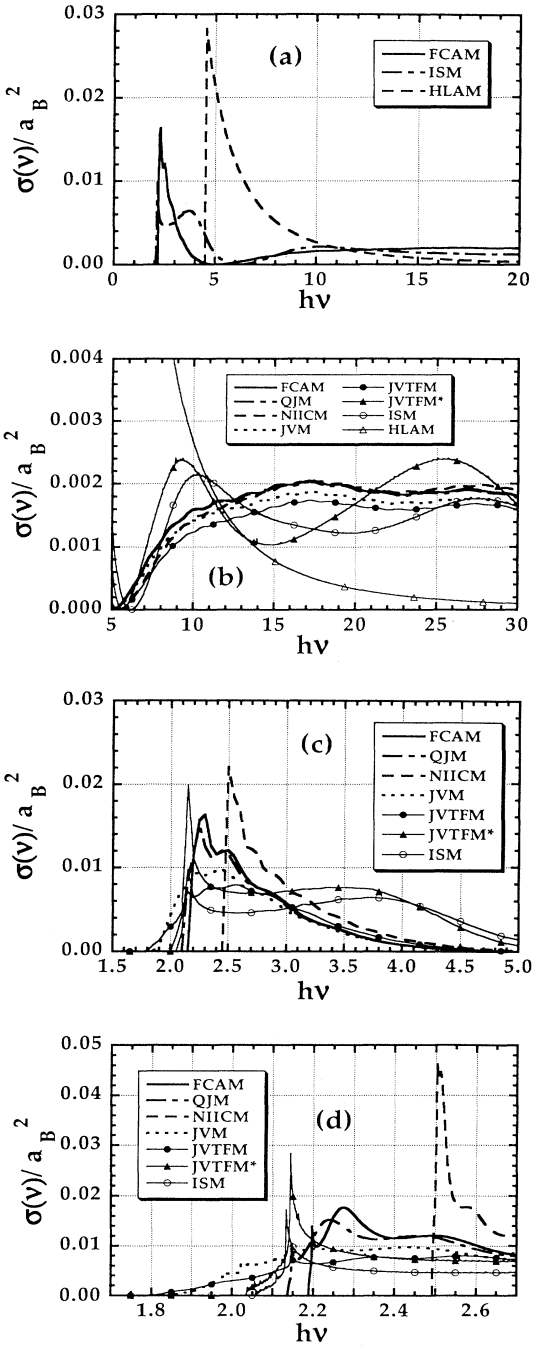

FIG. 8. (a) The photoionization cross section for case 2. All lines have the same meaning as in Fig. 3(a). (b) The photoionization cross section for case 2. All lines have the same meaning as in Fig. 3(b). (c) The photoionization cross section for case 2. All lines have the same meaning as in Fig. 3(c).

observe that a small enough increment of the photon energy around roughly 0.002 reveals the existence of threshold.

Figure 4 shows the number density of states defined by Eq. (3.6). In Fig. 4(a) the number densities of states by FCAM, QJM, NIICM, JVM, and JVTFM are shown. The five lines have the same meaning as those in Fig. 3(c). In Fig. 4(b) the number densities of states by JVTFM* and ISM are shown. The solid line represents that by JVTFM* and the dashed line that by ISM. As shown in Fig. 4, they have almost the same photon energy dependence, except for the location of the threshold. Differences between the absolute values in 4(a) and of those in 4(b) originate from the normalization conditions of the wave functions of free states.

Figure 5 shows the dipole integral defined by Eq. (3.3). For the meaning of the lines and parts 5(a) and 5(b) refer to Fig. 4. As shown in Fig. 5, their photon energy dependencies are quite different; one can see that the structures of the photoionization cross section are mainly affected by the dipole integrals. Figure 6 shows the wave function of free states with the electron kinetic energy $\varepsilon_\alpha=2.277\times10^{-3}$, 6.277×10^{-3}, and 0.05, respectively, and the wave function of the $1s$ state by HLAM. In Fig. 6, 1) correlations to the case $\varepsilon_\alpha=2.277\times10^{-3}$, 2) to the case $\varepsilon_\alpha=6.277\times10^{-3}$, and 3) to the case $\varepsilon_\alpha=0.05$. Case 1) indicates the behaviors near the threshold of photoionization cross sections by FCAM, case 2) at near the peak-value photon energy by FCAM, and case 3) at $h\nu=2.95$. In Fig. 6(a) I show the wave functions by FCAM, in Fig. 6(b) those by QJM, and in Fig. 6(c) those by JVTFM. As shown in Fig. 6(a), results in cases 1) and 2) are quite different and those of 1) and 3) are similar at the range of $r\lesssim3$. In case 2) the superposed wave function of free and bound states is larger than that in cases 1) and 3). This reflects the sharpness of the photoionization cross section near the threshold by FCAM.

In Fig. 7, the photoionization cross sections for case 2 are shown. Parts 7(a), 7(b), 7(c), and 7(d) are the same as in Fig. 3. As shown in Fig. 7(b), the photoionization cross sections increase oscillating as the photon energy increases. In case 1, they oscillate around a value, not increasing. As shown in Figs. 7(c) and 7(d), the structure of the photoionization cross sections near the threshold is similar to those in case 1. One can see that the photoionization cross section by NIICM has the sharp peak in Fig. 7(d).

In Fig. 8, the photoionization cross sections for case 3 over shown. Here also parts 8(a), 8(b), 8(c), and 8(d) are the same as in Fig. 3. As shown in Fig. 8(b), those by JVTFM* and ISM oscillate with large amplitude. In case 1, they oscillate around a value with small amplitude. As shown in Figs. 8(c) and 8(d), the structure of the photoionization cross sections by FCAM and QJM are almost the same. This reflects the fact that in case 3 the ion-ion correlation effects on the photoionization cross section are larger than the free-electron–free-electron correlation effects because of high density.

C. The rate coefficients of photoionization

The rate coefficients of photoionization are estimated as a function of the photon temperature $T_{\rm ph}$ by integrating Eq. (3.11) at the range from $h\nu=0$ to 30 with $\Delta h\nu=0.05$. Their values are summarized in Table II. Figure 9 shows the photon distribution functions for different photon temperatures: 10, 20, 30, 40, and 50 eV. The horizontal axis denotes the photon energy and the vertical axis $F(h\nu)$ defined by Eq. (3.13). As the photon temperature decreases, the shape of the distribution function becomes narrower and the values are reduced. Figure 10 shows the rate coefficients of photoionization normalized by that of ISM as a function of the photon temperature. It is defined by

TABLE II. Rate coefficient (s^{-1}) of photoionization as a function of the photon temperature $T_{\rm ph}$ (eV).

$T_{\rm ph}$	FCAM	QJM	NIICM	JVM	JVTFM	JVTFM*	ISM	HLAM
			Case 1: $Z=3$, $\bar{n}_i=5\times10^{22}$ cm^{-3}, and $T=50$ eV					
10.0	3.075×10^{6}	2.538×10^{6}	7.509×10^{5}	5.132×10^{6}	5.152×10^{6}	4.781×10^{6}	4.815×10^{6}	1.880×10^{5}
20.0	2.477×10^{8}	2.157×10^{8}	1.038×10^{8}	3.791×10^{8}	3.822×10^{8}	4.009×10^{8}	4.001×10^{8}	1.724×10^{8}
30.0	1.184×10^{9}	1.053×10^{9}	5.979×10^{8}	1.750×10^{9}	1.768×10^{9}	1.931×10^{9}	1.920×10^{9}	1.943×10^{9}
40.0	2.869×10^{9}	2.591×10^{9}	1.622×10^{9}	4.085×10^{9}	4.129×10^{9}	4.587×10^{9}	4.562×10^{9}	7.046×10^{9}
50.0	5.424×10^{9}	4.970×10^{9}	3.359×10^{9}	7.375×10^{9}	7.450×10^{9}	8.337×10^{9}	8.306×10^{9}	1.603×10^{10}
			Case 2: $Z=4$, $\bar{n}_i=5\times10^{22}$ cm^{-3}, and $T=50$ eV					
10.0	9.071×10^{3}	8.748×10^{3}	4.039×10^{3}	5.109×10^{4}	4.828×10^{4}	3.738×10^{4}	3.559×10^{4}	2.538×10^{1}
20.0	1.758×10^{7}	1.705×10^{7}	1.140×10^{7}	5.675×10^{7}	5.507×10^{7}	5.089×10^{7}	4.969×10^{7}	2.777×10^{6}
30.0	2.398×10^{8}	2.326×10^{8}	1.752×10^{8}	6.343×10^{8}	6.215×10^{8}	6.098×10^{8}	5.982×10^{8}	1.547×10^{8}
40.0	9.269×10^{8}	8.992×10^{8}	7.171×10^{8}	2.211×10^{9}	2.177×10^{9}	2.198×10^{9}	2.160×10^{9}	1.241×10^{9}
50.0	2.176×10^{9}	2.114×10^{9}	1.743×10^{9}	4.838×10^{9}	4.779×10^{9}	4.907×10^{9}	4.824×10^{9}	4.519×10^{9}
			Case 3: $Z=3$, $\bar{n}_i=2\times10^{23}$ cm^{-3}, and $T=50$ eV					
10.0	1.642×10^{7}	1.742×10^{7}	8.723×10^{6}	2.103×10^{7}	1.814×10^{7}	2.124×10^{7}	1.350×10^{7}	1.880×10^{5}
20.0	5.534×10^{8}	5.679×10^{8}	4.177×10^{8}	6.125×10^{8}	5.723×10^{8}	7.926×10^{8}	5.839×10^{8}	1.724×10^{8}
30.0	2.041×10^{9}	2.077×10^{9}	1.708×10^{9}	2.183×10^{9}	2.110×10^{9}	3.268×10^{9}	2.581×10^{9}	1.943×10^{9}
40.0	4.394×10^{9}	4.453×10^{9}	3.828×10^{9}	4.617×10^{9}	4.512×10^{9}	7.459×10^{9}	6.107×10^{9}	7.046×10^{9}
50.0	7.754×10^{9}	7.841×10^{9}	6.863×10^{9}	8.050×10^{9}	7.859×10^{9}	1.338×10^{10}	1.124×10^{10}	1.603×10^{10}

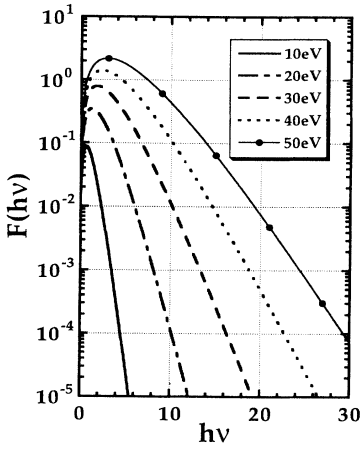

FIG. 9. The photon distribution function for different photon temperatures: 10, 20, 30, 40, and 50 eV. The horizontal axis denotes the photon energy and the vertical axis $F(h\nu)$ is defined by Eq. (3.13).

$$A_R(T_{\rm ph}) = A(T_{\rm ph})/A_{\rm (ISM)}(T_{\rm ph}) . \quad (4.1)$$

As shown in Figs. 10(a) and 10(b), which correspond to cases 1 and 2, differences of the A_R value reflect different treatments of the ion-ion correlation effect. Also in Fig. 10(b), differences of the normalization conditions of the wave function of free states affect the rate coefficients at $T_{\rm ph}=10$ eV. In case 3, as shown in Fig. 10(c), all of the particle correlation effects affect the rate coefficients with comparable magnitude, but in a complex way. Accuracy of the estimation of the electronic states of an atomic in hot dense plasmas greatly affects the rate coefficients of photoionization. Figure 11 shows the rate coefficients of photoionization by FCAM, ISM, and HLAM in cgs units. As shown in Fig. 11(a), which corresponds to case 1, the rate coefficient by FCAM is roughly 15 times that of HLAM at $T_{\rm ph}=10$ eV and roughly 0.35 times that of HLAM at $T_{\rm ph}=50$ eV. As shown in Fig. 11(b), which corresponds to case 2, the rate coefficient by FCAM is roughly 400 times that of HLAM at $T_{\rm ph}=10$ eV and roughly 0.5 times that of HLAM at $T_{\rm ph}=50$ eV. Finally, in Fig. 11(c), which corresponds to case 3, the rate coefficient by FCAM is roughly 100 times that of HLAM

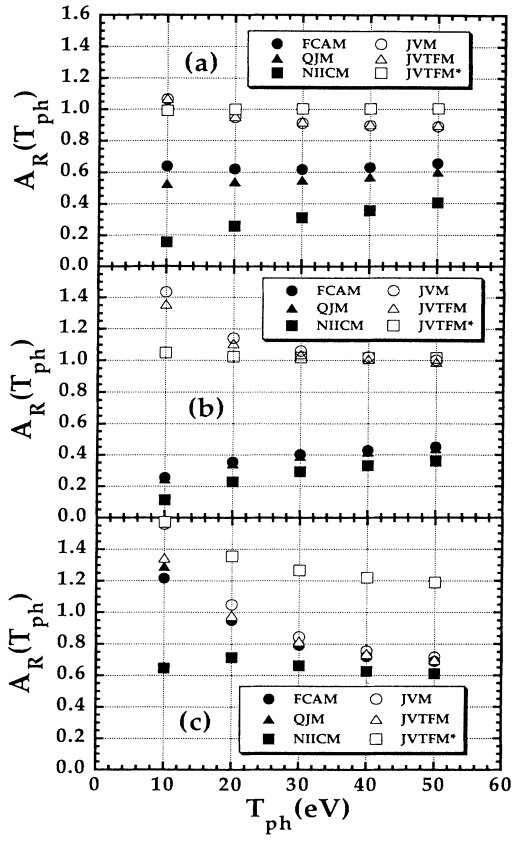

FIG. 10. (a) The rate coefficients of photoionization normalized by that of ISM as a function of the photon temperature $T_{\rm ph}$ defined by Eq. (5.1) for case 1. (b) The same as (a) except those that are obtained for case 2. (c) The same as (a) except those that are obtained for case 3.

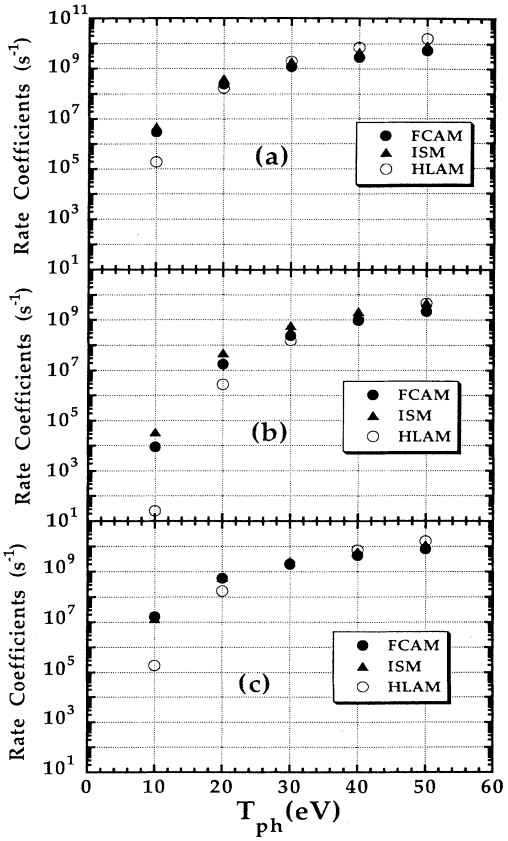

FIG. 11. (a) The rate coefficient of photoionization by FCAM, ISM, and HLAM in cgs units for case 1. (b) The same as (a) except for case 2. (c) The same as (a) except for case 3.

at $T_{ph}=10$ eV and roughly 0.5 times that of HLAM at $T_{ph}=50$ eV. As mentioned above, the interparticle correlation effect strongly affects the rate coefficients of photoionization.

V. CONCLUDING REMARKS

The cross sections and the rate coefficients of photoionization in hot dense plasmas are estimated quantitatively by using the atomic model presented in the previous work [2], which are compared with those obtained by other models for three cases mentioned in the preceding section. The energy level of the $1s$ state ε_{1s} is larger than that of hydrogenlike atom approximation. The wave functions of free states affect considerably the cross section and the rate coefficient of photoionization. It is shown that the photoionization cross sections have fine structures which are mainly determined by the wave functions of free states. In case 1, where a set of parameters is $Z=3$, $\bar{n}_i=5\times10^{22}$ cm^{-3}, and $T=50$ eV, the rate coefficient by FCAM is roughly 15 times that of HLAM at $T_{ph}=10$ eV and roughly 0.35 times that of HLAM at $T_{ph}=50$ eV. In case 2 , where a set of parameters is $Z=4$, $\bar{n}_i=5\times10^{22}$ cm^{-3}, and $T=50$ eV, the rate coefficient by FCAM is roughly 400 times that of HLAM at $T_{ph}=10$ eV and roughly 0.5 times that of HLAM at $T_{ph}=50$ eV. In case 3, for a set of parameters $Z=3$, $\bar{n}_i=2\times10^{23}$ cm^{-3}, and $T=50$ eV, the rate coefficient by FCAM is roughly 100 times that of HLAM at $T_{ph}=10$ eV and roughly 0.5 times that of HLAM at $T_{ph}=50$ eV. As mentioned in the preceding section, the interparticle correlation effects affect significantly the photoionization cross section in hot dense plasmas. I thus conclude that it is quite important to analyze the electronic states with good precision for the estimation of photoionization in hot dense plasmas.

ACKNOWLEDGMENTS

I wish to thank Professor K. Fujima, Professor T. Fujimoto, and Dr. S. Kato for useful discussions on photoionization. My thanks go also to Professor K. Nishihara, Professor S. Nakai, and Professor C. Yamanaka for their interest and encouragement.

[1] D. Salzmann, R. Y. Yin, and R. H. Pratt, Phys. Rev. A **32**, 3627 (1985).
[2] H. Furukawa and K. Nishihara, Phys. Rev. A **46**, 6596 (1992).
[3] J. Chihara, Prog. Theor. Phys. **72**, 940 (1984), and references therein.
[4] B. F. Rozsnyai, J. Quant. Spectrosc. Radiat. Transfer **13**, 1285 (1973).
[5] For example, F. Herman and S. Skillman, *Atomic Structure Calculations* (Prentice-Hall, Englewood Cliffs, NJ, 1963).
[6] M. Ishitobi and J. Chihara, J. Phys. Condens. Matter **4**, 3679 (1992).
[7] F. Perrot and M. W. C. Dharma-wardana, Phys. Rev. A **30**, 2619 (1984).
[8] B. F. Rozsnyai, Phys. Rev. A **5**, 1137 (1972).
[9] Donald H. Menzel and Chaim L. Pekeris, *Absorption Coefficients and Hydrogen Line Intensities* (The Royal Astronomical Society, London, in press).